Artificial Tactile Sensor Structure for Surface Topography Through Sliding

Kwonsik Shin, Minkyung Sim, Eunmin Choi, Hyunchul Park, Ji-Woong Choi, *Senior Member, IEEE*, Yuljae Cho, Jung Inn Sohn, Seung Nam Cha, and Jae Eun Jang

***Abstract*—Tactile sensors mimicking the human sense of touch have been studied and various technologies for the sensing of external stimuli have been suggested as well. Humans detect certain external stimuli and become aware of related sensations, such as roughness or smoothness. Among the various physical parameters, surface information is the most informative type of perception to impart these sensations onto an electromechanical system, such as an android robot or a smart phone. Here, an array sensor, which uses a sliding method for the precise perception of surface information, such as shapes and structures, is demonstrated. The suggested array sensor design with the excellent dynamic response of a piezoelectric material results in enhanced spatial resolutions with sliding motions and detects variable sliding speeds. A soft material was employed to the sensor to enhance the capability of shape distinction. Color mapping was applied to translate surface patterns into visual images. The reconfigured surface information had high accuracy compared to actual information. The demonstrated sliding speed, pattern detection, and shape detection capabilities as well as the higher spatial resolutions allow the sensor to be utilized as an artificial tactile sensor.**

***Index Terms*—Piezoelectric device, polyvinyledenedifluoride-trifluoroethylene (PVDF-TrFE), shape detection, soft material, surface topography, tactile sensor.**

Manuscript received December 6, 2017; revised May 3, 2018 and August 8, 2018; accepted September 4, 2018. Date of publication September 19, 2018; date of current version December 13, 2018. Recommended by Technical Editor Cagatay Basdogan. This work was supported by the Samsung Research Funding Center of Samsung Electronics under SRFC-IT1501-03. *(Corresponding author: Jae Eun Jang.)*

K. Shin, M. Sim, E. Choi, J.-W. Choi, and J. E. Jang are with the Department of Information and Communication Engineering, Daegu Gyeongbuk Institute of Science and Technology, Daegu 711-873, South Korea (e-mail: ksshin@dgist.ac.kr; mksim@dgist.ac.kr; eunminchoi@dgist.ac.kr; jwchoi@dgist.ac.kr; jang1@dgist.ac.kr).

H. Park is with the Department of CH CS HVM, ASML Korea, Hwasung 18449, South Korea (e-mail: hyunchul9106@naver.com).

Y. Cho is with the Department of Electrical Engineering Science, University of Oxford, Oxford OX1 3PJ, U.K (e-mail: yuljae.cho@eng.ox.ac.uk).

J. I. Sohn is with the Division of Physics and Semiconductor Science, Dongguk University-Seoul, Seoul 04620, South Korea (e-mail: junginn.sohn@donguguk.edu).

S. N. Cha is with the Department of Physics, Sungkyunkwan University, Suwon 16419, South Korea (e-mail: chasn@skku.edu).

Color versions of one or more of the figures in this paper are available online at http://ieeexplore.ieee.org.

Digital Object Identifier 10.1109/TMECH.2018.2870917

I. Introduction

THE mimicking of the five human senses has been one of the most interesting areas of study in relation to engineering thus far. Research on hearing and sight has long been conducted, resulting in the inventions of the recorder, audio devices, the camera, and the television. These mimicking devices have had profound effects on human societies. However, there remain numerous issues with regard to the sense of touch. Touch is related to various external stimuli, such as pressure, temperature, vibration, tension, shear force, and others. Many types of tactile receptors respond to external stimuli and create an electrochemical signal known as an action potential [1]. The electrochemical signal is sent to the brain and the human is then able to feel a sense of touch [2]. Recently, some groups have studied sensors, which mimic tactile receptors. For example, capacitive [3], piezoelectric [4], [5], piezoresistive [6], and pyroelectric [7] types of sensors have been studied for their ability to detect pressure levels and temperatures. Such sensors can be applied as functions of mechanoreceptors and thermoreceptors [8]. Various sensor structures have been considered for high sensitivity, high resolutions, and multitouch capabilities, as well as flexibility and stretchability [9]. However, artificial tactile sensors cannot yet match the human sense of touch perfectly because humans feel not only external physical stimuli, such as pressure and temperature, but also psychological parameters, such as roughness, smoothness, hardness, and even pain through the sense of touch. Recently, psychological interfaces between humans and artificial systems have received attention [4], [10]. Among these psychological tactile feelings, roughness, and smoothness have been the most difficult feelings to mimic, as people have different criteria for sensing these psychological parameters [11]. Despite the many issues pertaining to which physical components are most informative for perceiving roughness or smoothness, it is indisputable that sensing a surface topography is the starting point to perceive feelings of roughness and smoothness. Unfortunately, there are relatively a few research results related to tactile sensors for surface information detection in comparison with those for pressure and temperature detection. One of the reasons behind this is related to how a robot holds an object with its fingers, a major concern in the android robot field. Despite this, many factors other than pressure and temperature should be considered when attempting to undertake surface information sensing [12]. In some studies, a robot finger

with a single pressure sensor slides the surface of an object and recognizes the surface shape using various principles based on a contact point analysis [13], a feedback loop [14], a flow chart [15], Gaussian statistics [16], and a spatial low-pass filter [17], [18]. However, the single sensor structure is limited in terms of its fundamental spatial resolution, and some coefficients or constant factors should be known in advance for data analysis. Moreover, the analysis principles require complex algorithms and programming to analyze the data. Piezophotonic and optical sensors can offer better surface sensing results, but these sensors require a light source and additional optical equipment, which can be a structural barrier for robot or other electronic device applications [19]. In this paper, we introduce a piezoelectric type of sensor array structure for surface topography and shape detection that works via a sliding process, similar to how a human operates. The sensor showed enhanced spatial resolutions with sliding condition. In addition, the sensor system can measure the sliding speed through a simple signal analysis, and when generating electrical signals, the surface topography can easily be reconfigured in a reverse manner. A soft material was also embedded in the sensor to distinguish clearly among different surface shapes. A slope analysis involving the summing of all integral values was conducted to investigate the depth information.

II. Background

A. Array Structure

Humans feel a surface topography in two ways: by touch and by sliding [20]. This highly sensitive surface perception is possible due to the array-type distribution of tactile receptors in the human skin. If humans had a single receptor, it would be difficult to feel complex stimuli, such as surface textures or roughness and smoothness. A robot finger based on a single sensor has been generally used in most robot applications thus far. The robot finger design requires a speedometer type of device, such as a gyroscope, to detect the surface shapes of certain objects, which is one disadvantage due to the structural difference from a human finger, besides the poor spatial detection sensitivity. Thus, a sensor array structure is desirable to mimic the human touch system for the sensing of surface topographies.

B. Piezoelectric Materials

Various sensor structures employing a piezoresistive, a capacitive, an electrical resistive, and a piezoelectric type of sensor have been studied for tactile sensors. A piezoelectric sensor is demonstrated here. Piezoelectric materials have the ability to generate electrical power as a response to applied stress [21]. According to physiological analysis, skin has properties similar to piezoelectric [22]. Accordingly, the mechanical and electrical properties of the piezoelectric materials are coupled with a linear relationship between the applied stress and internal electric polarization. The resulting charge displacement D_i induced by the applied stress is defined as

$$D_i = \varepsilon_{ik} E_k + d_{im} \sigma_m \tag{1}$$

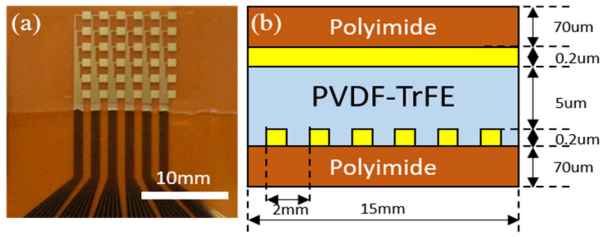

Fig. 1. Image of (a) piezoelectric sensor array and (b) cross-section depiction of the sensor. A transparent layer upon the array design indicated in (a) is the coated piezoelectric film.

where ε_{ik} is the dielectric permittivity, E_k is the electric field, d_{im} is the piezoelectric coefficient, and σ_m represents the components of the stress tensor. Since the suggested array sensor is connected to data acquisition system (DAQ) directly to analysis the piezoelectric signals, any electrical sources (reference voltage, charge, and field) were not applied in the study. So, E_k is negligible. The electric displacement can be defined as

$$D_i = d_{im}\sigma_m = \frac{q_{\text{sensor}}}{A_{\text{piezo}}} = \frac{C_p \cdot V_p}{A_{\text{piezo}}} \tag{2}$$

where q_{sensor} is the electric charge generated by the sensor and A_{piezo} is the loaded piezoelectric area. Because the piezoelectric charge q_{sensor} versus the stress applied on the piezoelectric surface can be expressed as $q_{\text{sensor}} = C_p \cdot V_p$ [23], a mathematical model of the piezoelectric voltage can, therefore, be described as follows:

$$V_p = \frac{A_{\text{piezo}}}{C} d_{im}\sigma_m = \frac{d_{im} \cdot A_{\text{piezo}}}{C}\sigma_m. \tag{3}$$

With this formula, the generated piezoelectric voltage is expressed as a function of the applied stress (i.e., $\sigma_m = \frac{F_m}{A_{\text{contact}}}$). More voltage signals can be generated with a high-piezoelectric-coefficient material, and the voltage can be directly measured with a measuring instrument. This is an important advantage for devices, which consume only low amounts of power. Although the sensor system requires an external power source for data acquisition and analysis, it can reduce power consumption due to the advantage of generating the signal itself. In addition, piezoelectric sensors are suitable for measuring dynamic responses owing to their high sensitivity and high frequency electromechanical bandwidth [20]. Specifically, sensors using piezoelectric copolymers such as polyvinyledenedifluoride-trifluoroethylene (PVDF-TrFE) are highly suitable due to their flexibility, simple fabrication processes, and high sensitivity levels [24].

C. Fabrication

For the array structure and the individual action of each cell, bottom electrodes were patterned by a photolithography process. The design of electrode patterning has 36 cells, with each cell 1 mm^2 in size with a 2 mm cell-to-cell pitch [see Fig. 1(a)]. Cr and Au (50 nm and 200 nm) were employed as the electrode materials, formed by a sputtering process. After the metal deposition step, a lift-off process was conducted to create an array structure. A PVDF-TrFE solution (15%) was formulated

TABLE I
CHARACTERISTIC COMPARISONS ON THE EXISTING AND THIS SENSOR

Type and array	Cell size (mm)	Pitch (mm)	Sensing method	The smallest detection size(mm)
Piezoresistive (12×8) [25]	3 × 3 × π	10	Touch	10
Capacitive (3×3) [26]	5 × 5	5	Sliding	-
Capacitive (2×2) [27]	3 × 3	5.5	Sliding	5.5
Proposed Piezoelectric (6×6)	1 × 1	2	Touch & sliding	0.2

by mixing PVDF-TrFE powder with 2-butanol as a solvent. The solution was then coated onto the patterned polyimide film by means of a spin-coating method at 3500 r/min in order to make thin piezoelectric material film, after which it was annealed for two hours at 130 °C in a conventional oven. The piezoelectric coefficient d_{33} of the PVDF-TrFE film is around 5.3 pC/N. A poling process was not performed here because the generated piezoelectric signal has an enough SNR value without a poling process. The thickness of the fabricated piezoelectric material layer was optimized to get high SNR and signal stability. The thicker the PVDF, the smaller the SNR. The thin PVDF layers had a high SNR values, but it was easily damaged. Therefore, the 5 μm thickness was used for the optimization in the study. For the top common electrode, Cr/Au was also deposited onto polyimide films by sputtering. Finally, the bottom substrate with PVDF-TrFE and the top electrode substrate were assembled via an alignment process to create a sandwich structure consisting of an electrode-piezo polymer electrode, which was then sealed. The total thickness of the array sensor was around 150 μm. The proposed sensor has a higher spatial resolution than current similar state-of-the-art devices. Table I shows that some sensors have a wider cell size and wider spacing distances than our sensor. Depending on the sensing mechanism and materials, sensing methods are limited as only touch or just sliding for other studies. However, the proposed sensor cannot only detect touch state and but also sliding signals due to the piezoelectric mechanism. When static force is applied on sensor, there are a dynamic press state and a release state before and after static force state, so that, the applied static forces could be detected by analyzing the peak levels and amplitudes of the generated signals of these two dynamic signal, although there is no signal during real static force state. As noted above, piezoelectric materials have a high sensitivity and a high frequency electromechanical bandwidth characteristics and can, therefore, be utilized as sensors for both static and dynamic motions. Our sensor has more enhanced spatial resolution characteristics than the sensor design value given the sliding effect, as will be demonstrated Section IV.

III. EXPERIMENTAL DETAILS

A. Sensor Characteristic

The basic points of sensor characteristics are important to understand well with regard to the main subject. The general characteristics of the sensor, such as reliability, sensitivity, linearity, hysteresis, and sliding signal changes depending on

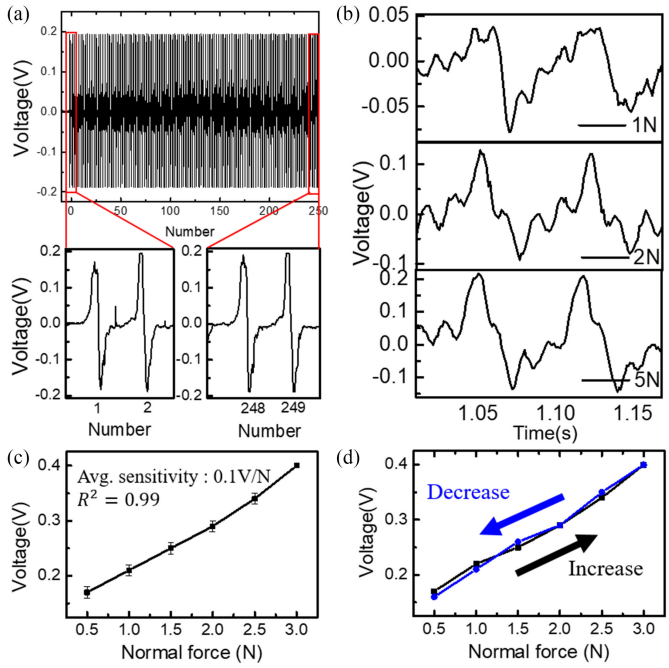

Fig. 2. General characteristics of (a) reliability, (b) sliding signals with different normal forces, (c) sensitivity and (d) hysteresis test of the sensor.

different normal forces were initially analyzed. To determine the reliability of the piezoelectric sensor, we were carried out a 250-cycle sliding test using a linear stage [see Fig. 2(a)]. The first and second sliding signals were compared with the last two signals. The results showed that the four signals have a similar signal waveform as well as voltage level, indicating that the sensor has a good reliability. Because this paper concentrates on both static and dynamic motions, we basically experimented with sliding signal changes depending on the different normal forces [see Fig. 2(b)]. Normal force values of 1–5 N were tested in order to find an appropriate value for both touch and sliding experiments. If we apply 5 N to the sensors, a higher SNR ratio can be obtained, but the sensor can be worn down quickly due to the excessive force. The voltage level for the 1 N condition had a relatively low SNR, and the signal was a little distorted due to the insufficient pressure. Considering the high SNR ratio and signal distortion points, 2 N was used to optimize the quality of the signal and for improved sensor protection. Besides, the 2 N condition was used as appropriate fixed test value considering the real human motion and the quality of signal characteristics in the study. The calibration curve (force versus output) was analyzed in order to measure the sensitivity and linearity of the sensor, as shown in Fig. 2(c) (touch case). A calibration graph of the sensor showed 0.1 V/N sensitivity with high linearity ($R^2 = 0.99$). The electrical hysteresis characteristic of the proposed sensor was not found [see Fig. 2(d)]. It is assumed that no polling process and low applied force level do not induce to well align state of dielectric dipoles in PVDF.

B. Touch Experiment

The characteristics of the sensing signals by the simple touch method were studied first. The array sensor was pressed by three

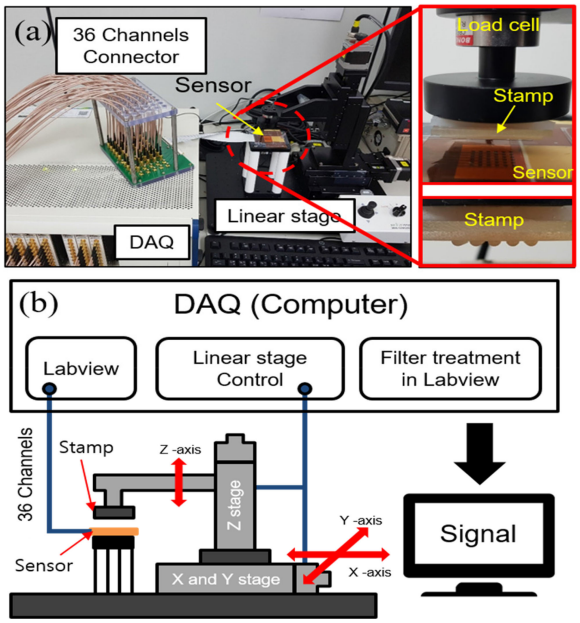

Fig. 3. Experimental setting. (a) Image of the experimental set-up. The sensor was connected to DAQ equipment. (b) Block diagram of the set-up. The DAQ is used to collect piezo signals while also controlling the linear stages and signal processing steps.

different test stamps in the shape of a square, a triangle, and a dome. Various stamps having different pitches were initially created by using a three-dimensional (3-D) printer, as noted above. Because of the system limits and reliability of 3-D printers, a 3-mm pitch was an appropriately smaller value with which to create various test stamps. Therefore, we chose 3 mm as the pitch for the test stamps. Young's modulus of the stamp material is around 3 GPa. The square and the dome shapes each had a width of 1 mm and a radius of 1 mm. The vertex of the triangle shape had a fine width of 0.2 mm due to the resolution limit of the 3-D printer. 2 N was applied by a linear stage as the pressing force to obtain a piezoelectric signal. The piezoelectric signals are measured and collected by data acquisition equipment (National Instruments) during the touch experiments. The sensor array and DAQ equipment were connected to each other using flexible flat cable (FFC) and SubMiniature version B (SMB) cables (see Fig. 3). The measured piezoelectric signal had an enough SNR level, so that the voltage or charge amplifier was not used. The generated piezoelectric signals were collected and then displayed in real time in the LABVIEW program. A 60-Hz FFT filter and a 10× amplification were used in this study. A 1 K/s sampling rate was used in all experiments because this sampling rate was rapid enough to cover various sliding speed conditions. The generated voltage generated is expressed in the color maps shown in Fig. 4. In spite of the identical force pressing conditions, the generated voltage differed due to contact area differences. Therefore, 0.4 V, the lowest value, was detected by the square stamp due to its large contact. On the other hand, 0.6 V was generated by the triangle stamp due to its small contact area [see Fig. 4(a) and (b)]. The sensor showed different output voltages depending on the shape of the stamp, but it is difficult to distinguish between different shapes of objects. This can be a major problem; for

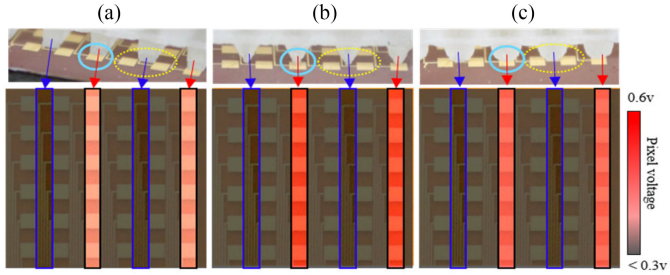

Fig. 4. Voltage mapping images of square, triangle, and dome shapes. The generated voltage increased corresponding to the shapes of the stamps, but there was still a resolution limit. (a) Square, (b) Triangle, (c) Dome.

example, if the sensor is pressed strongly by the square stamp, it cannot distinguish whether it is a square or a triangle. To detect a difference in the shape via the simple touching method, the resolution of the sensor should be higher than that of the touched object. If the dimensions of a single sensor are larger than the dimensions of the detected objects, the final output data from the sensors will have missing or distorting information with regard to the original shape of the touched object [28], [29]. Some parts of stamp cannot be detected by the sensor as like blue box case in Fig. 4. This indicates that it is not easy to detect different shapes perfectly using the simple touch method. A spatial low-pass filer can be used as an antialiasing filter for limited tactile spatial [18]. This treatment has been utilized to improving the resolutions of pressure distributions. However, the main purpose here is to understand piezoelectric signals with sliding motions for detecting surface topographies; therefore, a filter treatment was not studied.

C. Sliding Experiment

Sliding is another means of surface topography detection. Humans can detect surface information well by the sliding motion of a finger, even if the size of the object touched is very small. Like the human finger, much smaller sensor designs can be achieved easily by using a microfabrication process but we would like to show that the sliding skill of the sensor can cover the detection of objects smaller than the sensor. Considering the fabrication limits of the test object formed by 3-D printing, we chose the 2 mm pitch condition as the sensor design value. The stamps were mounted on linear stages and were then moved onto the sensor array at a rate of 30 mm/s. We set the linear stage and load cell to apply 2 N to the sensor by a software in advance. The total force applied to the sensor is a vector value that combines the sliding motion (30 mm/s) and normal force (2 N). Since the sliding motion is added, the total force increases slightly. Fortunately, all sliding conditions for various shape are the same. We may need a simple correction when surface information is detected by the piezoelectric voltage. However, the piezopeak position on time domain is main parameter, so that the correction of voltage value cannot be required. Piezoelectric signals by sliding were detected, as shown in Fig. 5. The lowest voltage arose with the square shape, and higher voltage signals by nearly 200% were detected with the triangle and dome shapes. Apart from the voltage levels, each sliding

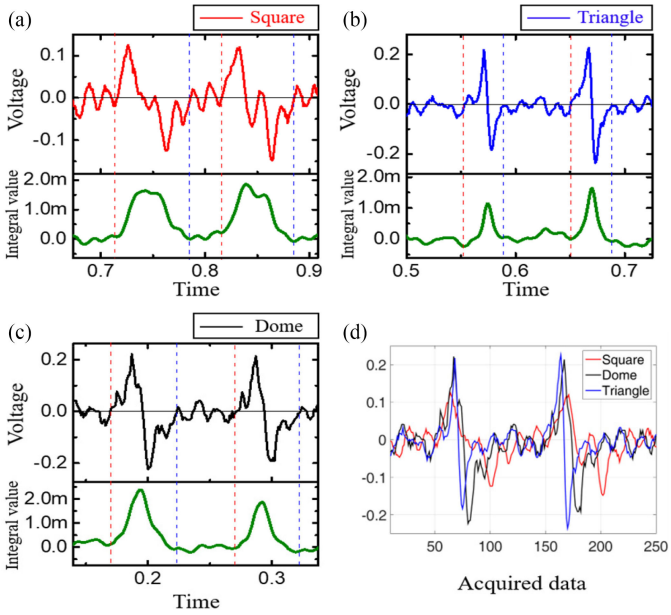

Fig. 5. Measured sliding signals of the different stamps. (a) Square. (b) Triangle. (c) Dome. The integral graphs (green signal) of the measured voltage signals were analyzed in a mechanism of the sliding signals.

signal differed slightly depending on the stamp used. The sliding signal of the square was broader and had a lower slope than those of the other signals [see Fig. 5(a)]. On the other hand, the signals of the triangle and the dome were narrower and had higher slopes as compared to the square signal [see Fig. 5(b) and (c)]. The detected signal waveforms were compared by a signal processing approach known as the correlation method in order to distinguish the shapes [see Fig. 5(d)]. A correlation is a statistical relationship between two instances of random data [30]. A correlation coefficient is a number that quantifies the correlation and dependence, meaning the statistical relationships between two observed data values. If two observed data values have N scalar observations, then the correlation coefficient is defined as

$$\rho(A,B) = \frac{1}{N-1}\sum_{i=1}^{N}\left(\frac{A_i-\mu_A}{\sigma_A}\right)\left(\frac{B_i-\mu_B}{\sigma_B}\right) \quad (4)$$

where μ_A and σ_A are mean and standard deviation of A, respectively, and μ_B and σ_B are also the mean and standard deviation of B. The correlation coefficient matrix of two data instances is the matrix for each pairwise variable combinatio,

$$R = \begin{pmatrix} 1 & \rho(A,B) \\ \rho(B,A) & 1 \end{pmatrix}. \quad (5)$$

With the correlation coefficient method, the signal relationships between square, triangle, and dome ($\rho(A,B)$, $\rho(A,C)$, $\rho(B,C)$) were calculated. The matching percentages between the signals are shown in Table II based on the coefficients. These results also demonstrate that the sliding signal of the square differs from those of the triangle and dome as shown by the high correlation value. This also means that something more is required to distinguish between triangle and dome signals, even when using the sliding mechanism.

TABLE II
CORRELATION COEFFICIENT METHOD

Correlations between different signals	Matching Percentage
Square (A) and Triangle (B)	24%
Square (A) and Dome (C)	21%
Triangle (B) and Dome (C)	88%

D. Mechanism Analysis of the Sliding Signals

The piezoelectric voltage signal and integral graphs of the voltage signal (the green graph in Fig. 5) were analyzed in an effort to understand the piezoelectric mechanism in the sliding condition, as the integral value is related to the generated piezoelectric charges for sliding. When stamps with different shapes are slid over a cell, the stamps start to apply some pressure to the cell. At that moment (the red dotted line of the time axis), a positive slope appears in the voltage graph. Subsequently, when a stamp is positioned inside of the cell, the highest amount of pressure is applied. Then, because the stamp is positioned away from the cell, the applied pressure decreases. The generated voltage and charge also decrease according to the reduced pressure. Finally, after the stamp passes through the cell body entirely, the voltage and integral values return to a neutral state (the blue dotted line). It was found that the time interval of a signal period differed in accordance with the object shape. For the square stamp, the time interval was longest at 0.0705 s due to its large contact area. On the other hand, the triangle object had the shortest time interval of 0.038 s due to its small contact area. The dome object was in the middle in terms of the interval, at 0.057 s. However, it is not easy to recognize the dimensions of an object through interval time differences directly because the sliding speed should be known in advance.

IV. RESULTS AND DISCUSSION

A. Sliding Speed Calculation

Because sliding motion is used in this study to detect surface information, the sliding speed is essential to reconstruct the surface topography from the detected signal graph in which time is the x-axis value. For a single sensor structure, a speedometer type of device such as a gyroscope is essential. However, several solutions are feasible for determining the sliding speed for an array-type sensor structure without a speedometer. When sensor arrays touch and slide over the surface of certain objects, or vice versa, piezoelectric signals are generated on all of the touched cells. Fig. 6(a) presents successive detected signals from B and C cells and a schematic diagram corresponding to sliding motion. The signals appeared in cell B first and then appeared in cell C in sequence when the object was slid. The sliding speed can be calculated by the simple equation of $\upsilon = L/T$, where T is the time interval between signals arising from cells B and C and L is the distance between the two cells. L is determined

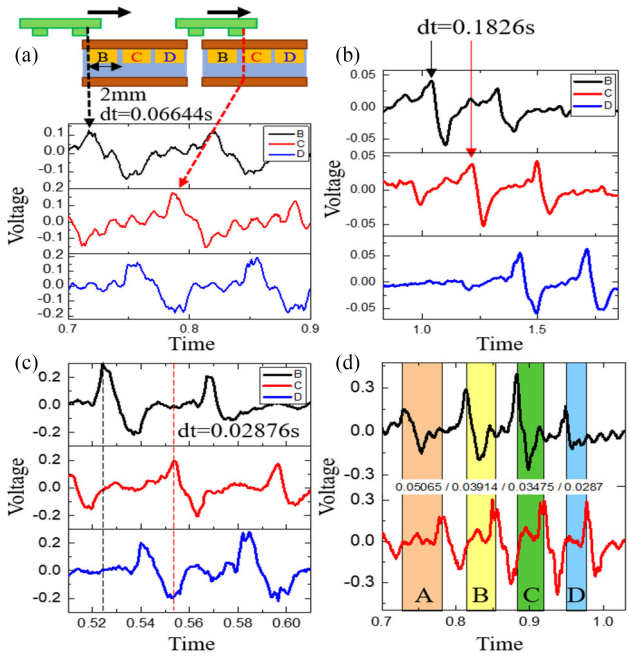

Fig. 6. Reverse calculation processes for sliding speed. (a) Mechanism of the sliding speed via the reversed calculation. The time interval of the sliding signals occurring in cells B and C and the distances between the cells were used for the speed calculation. (b) Piezoelectric signals at 10 mm/s sliding speed. (c) Piezoelectric signals at 70 mm/s sliding speed. (d) Calculate sliding speeds in random sliding speed condition.

according to the design geometry of the sensor array, and here it is fixed at 2 mm. T is measured by two positive peak points from cells B and C. The detected time in Fig. 6(a) is 0.06644 s. Therefore, the calculated speed was 30.1 mm/s. This value is in good agreement with the actual sliding speed of the linear stage. We conducted an experiment with various speeds ranging from 10 to 70 mm/s for signal optimization. This range was selected because speeds of 10–70 mm/s are similar to the sliding motion speed of human touch when feeling a texture. The sliding speeds of the linear stage were set to 10 mm/s and 70 mm/s, respectively, and the generated signal was then measured in order to extend the speed measurement capability [Fig. 6(b) and (c)]. The time intervals were 0.1826 s and 0.02876 s in the 10 mm/s and 70 mm/s conditions, respectively, and the corresponding calculated speeds were 10.95 mm/s and 69.54 mm/s. As under the 30 mm/s speed, the signal had a low SNR [see Fig. 6(b)], whereas around 70 mm/s, some aspects of the signal were slightly distorted [see Fig. 6(c)]. For this reason, we settled on 30 mm/s speed as other experimental condition. In addition, we identified that there is a voltage difference according to changes in the speed. The applied force was fixed at 2 N, but the pressing times of the 10 and 70 mm/s conditions were different. The increase in the piezoelectric charge per unit time in the 70 mm/s condition is much higher than that in the 10 mm/s condition; hence, a relatively high piezoelectric voltage appeared. Fig. 6(d) shows that the sensor can measure a random speed condition as well. The measured time intervals were changed continuously from 0.05065 s, 0.03914 s, 0.03475 s, and 0.02870 s and the calculated speeds were 39.49 mm/s, 51.09 mm/s, 57.55 mm/s, and 69.69 mm/s, respectively. The sensor was able not only to measure the changing speed capably, but the calculated values were also in good agreement with the actual speeds of the test system. Table III shows average value of calculated speed for 10 time slidings with sliding speed change.

TABLE III
SLIDING SPEED MEASUREMENT ON THE RANDOM SPEED CONDITION

	A region	B region	C region	D region
Time interval(s)	0.050	0.040	0.035	0.029
Calculated speed (mm/s)	40	50	57.14	68.96

B. Pitch Calculation and High-Resolution Characteristics

By calculating the sliding speed, the geometry of the object can be detected. The first square tip pressed cell B and the second tip also then passed cell B in sequence. Thus, piezoelectric signals appeared sequentially in cell B. The time interval of the two signals contains geometrical information pertaining to the two square structures, i.e., the pitch between the square structures. The sliding speed (υ) was calculated and determined to be 30.1 mm/s, as before, and the time interval between two peaks arising from cell B (T) was measured and found to be 0.099 s. The calculated pitch was found in this way to be 2.98 mm, very close to the pitch of the actual dimensions, at 3 mm. Thus, the geometrical factor for the x-axis can be detected precisely. One of the important advantages of the array-type sensor with the sliding method is that it can detect much higher resolutions than the resolution of the sensor. With only the simple touch method, the sensor cannot feasibly detect certain objects with smaller dimensions or higher spacing resolutions than those of the sensor array. We already noted this somewhat in the explanation of Fig. 4. To verify the capability of the array sensor with the sliding method for object shapes with higher resolutions, a pattern master with various pitches was fabricated with a 3-D printer. The thin line patterns have a pitch of 0.5–2.5 mm. The geometric details and a photograph of the random pitch matter are indicated in Fig. 7(c) and the experimental results are shown in Fig. 7(d). Although the dimensional pitch of the sensor array is 2 mm, the sensor arrays could detect higher resolutions well, as shown in Table IV. For example, the corresponding time intervals for the 0.5, 1, and 1.5 mm pitches were 0.017, 0.031 and 0.05 s, and we recalculated the pitch of the pattern master. Accordingly, the calculated pitches were 0.51 mm, 0.93 mm and 1.5 mm, respectively. These values were close to the actual values. This outcome is quite similar to the case of a human, with sensing ability for much smaller objects. We conducted an additional experiment to determine what would arise if the sliding direction is not along the x-axis. The stamp was tilted with the x- and y-axis and then was slid along the sensor [see Fig. 8(a)]. As the stamps slid in the diagonal direction, the order in which the signals appeared became somewhat complicated. However, the sensor suitably detected the signal generation order. First, cell B came into contact with the stamp, after which cell A did so after

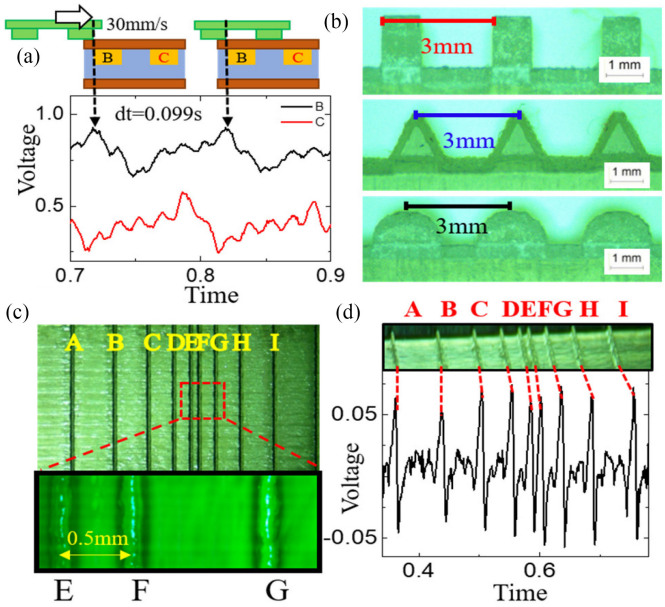

Fig. 7. Pitch calculation mechanism. (a) Time interval of the sliding signals in the same cell and the calculated speed were used for the pitch calculation. (b) Photographs and design of the different stamps. (c) Enlarged photographs of the random pitch stamp. (d) Successive sliding signals of a random pitch stamp (0.5–2.5 mm) in the 30 mm/s.

TABLE IV
TIME INTERVAL AND PITCH COMPARISON

	A to B	B to C	C to D	D to E
Time Interval	0.08s	0.067s	0.05s	0.031s
Calculated Pitch	2.4mm	2mm	1.5mm	0.9mm
Actual Pitch	2.5mm	2mm	1.5mm	1mm
	E to F	F to G	G to H	H to I
Time Interval	0.017s	0.034s	0.05	0.068
Calculated Pitch	0.5mm	1mm	1.5mm	2mm
Actual Pitch	0.5mm	1mm	1.5mm	2mm

0.05 s. As in Fig. 8(b), the peak of cell A (black) appeared after the peak of cell B (red). Because the contact distance in which the signals come in contact with the stamp differs, time intervals appears when the signal is generated and the time intervals could be accurately measured [see Fig. 8(b)]. From the results and the calculation method used earlier, the angle of the tilted stamp could be calculated [see Fig. 8(c)]. With this calculated sliding angle and an identical configuration, we can detect the surface topography well, as in the simple x-axis sliding case.

C. Surface Topography

We discussed in brief, the contact area of the objects in the section describing the mechanical analysis of the sliding signals (see Fig. 5), and the pitch of the objects was outlined in the section describing the sliding speed calculation (see Fig. 7) as well. In this section, surface topography is reconfigured using the previous results. The beginning and end of the piezoelectric signals indicate that the object starts and stops pressing a cell, respectively. Therefore, the time interval between the beginning and the end of the signal corresponds to the sum of the dimensions of the cell size and the width of the object. However, it is not easy to define a starting and an ending point of a signal when measuring it due to noise, implying that errors can arise. If based on the positive and negative peak points of piezoelectric signals, the measurement should be clearer, because the peaks are related to the pressing and the release states of a cell depending on the object. The sliding signals data were changed to absolute values to measure the time interval between the positive and negative peaks easily. The area under pressure is related to the contact area with the sensor, that is, the widths of the three different shapes. For the square shape, time intervals of 0.03664 and 0.03223 s were measured. The contact widths of the two squares were around 1 mm by multiplying the sliding speed. The calculated widths were well matched to the actual values. The dimensional information when touching the width is expressed in red. On the other hand, nonpressure areas are expressed in blue (see Fig. 9). The signal result of the triangle shape had the lowest time intervals of 0.0073 and 0.0069 s due to the narrow width of the vertex of the triangle shape. The width of the triangle shape also was calculated, resulting in a value of 0.2 mm, and the actual tip diameter of the vertex was around 0.2 mm. The calculated width of the dome shape was 0.4 mm. originally the dome shape should have a small contact width due to its curved surface. However, the dome shape formed by the 3-D printer could not have a perfectly curved surface due to the resolution limit of the 3-D printer. The 3-D printed dome shape had an actual contact width of 0.4 mm, and the contact width was close to the calculated width of the dome-shaped object. However, this calculation method is not feasible with depth-direction information because it is only was related to the contact width. Thus, for example, it may be difficult to distinguish between a 0.4 mm square and the dome tips. Hence, the sensor is still limited when used to distinguish between these different types of shapes. Although the sensor cannot yet distinguish between shapes perfectly in 3-D, it can represent the surface characteristics of certain objects, such as the width and pitch, with high accuracy. We undertook a sliding experiment with complex geometry stamps with square, triangle, and dome shapes in series. Previous stamps had a 3 mm pitch, but the complex stamp had random spacings between the features. Identical signal processing and calculation mechanisms were used for topography reconfiguration. Sliding signals corresponding to different shapes were measured and contact widths were well matched as well [see Fig. 9(d)]. The reconfigured images in Fig. 9 mainly include 2-D information, in this case the width and pitch, and not 3-D information (depth). However, we think that the measured parameters even in 2-D are important, as the precise detection of those factors on a 2-D plane is a primary step in the determination of the surface topography. The detected 2-D information, a simple shape detection method, and higher spatial resolutions are required to understand the surface properties. For the experiment, 0.2 mm object shape was detected by sliding motion of piezoelectric sensor with 1 mm^2 dimension and 1 mm spacing design. It means that the sensor can detect

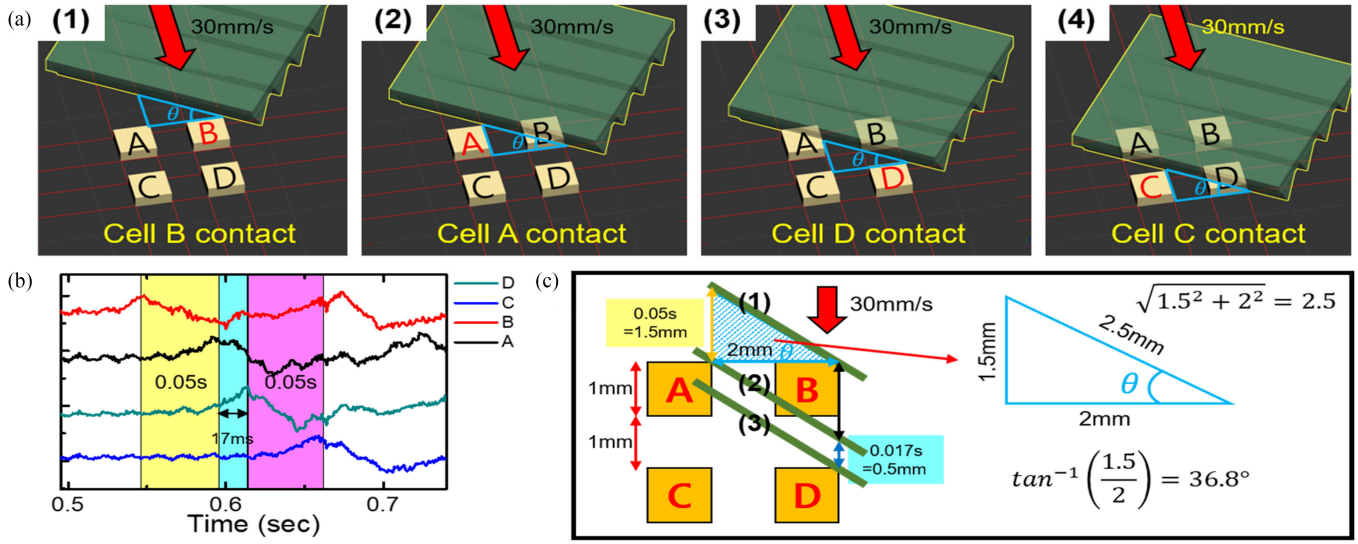

Fig. 8. Recalculation mechanism in the tilted case. (a) Schematic of the sliding motion with a tilted stamp. As the stamps slide in the diagonal direction, the order in which the signals appear becomes somewhat complicated. (b) Result of the sliding motion in the diagonal direction. (c) Top view schematic of the tilted case and the angle calculation mechanism.

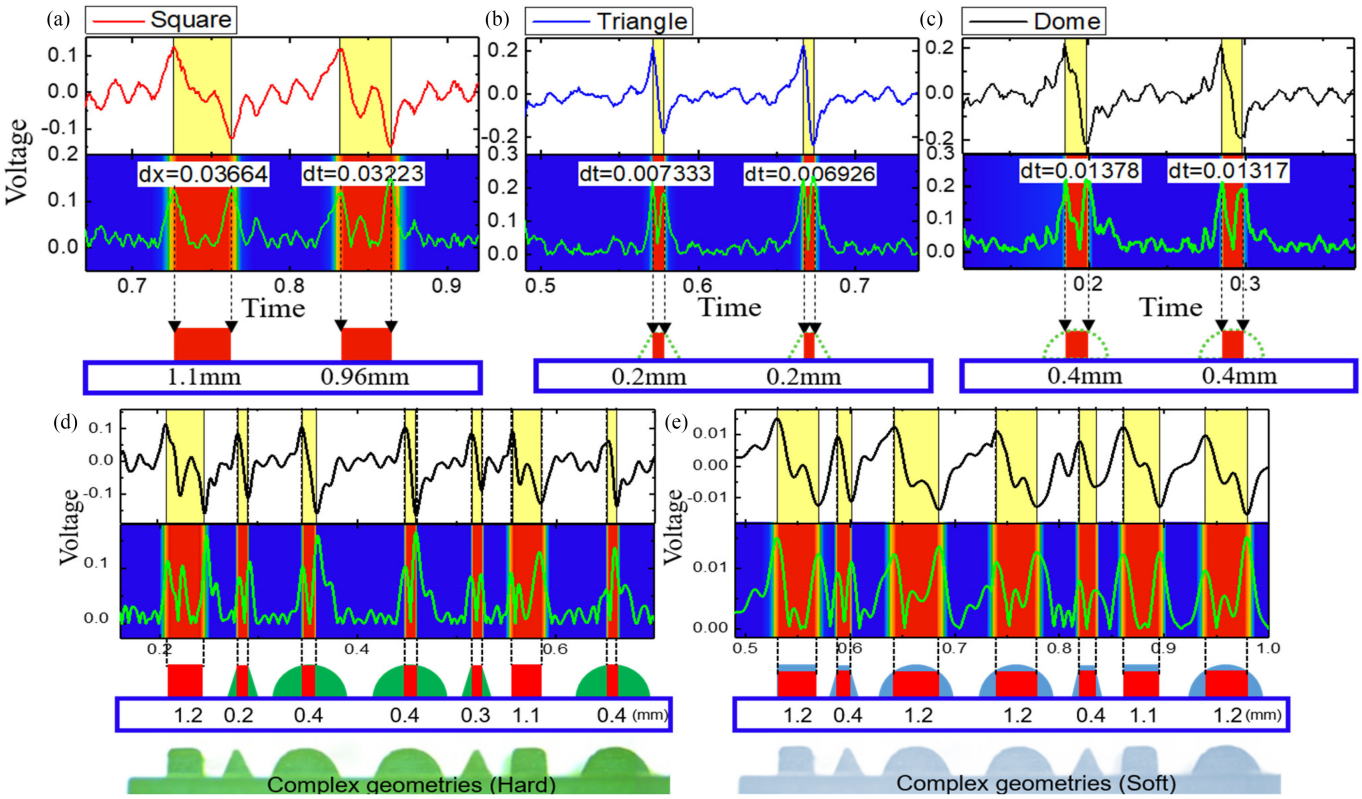

Fig. 9. Representation of the surface topographies from the sliding signals. The width of the shapes was related with the time interval between positive and negative peaks. The calculated widths of the three different shapes were very close to the actual values. Surface topographies are expressed by a color mapping to represent pressed and nonpressed areas. However, without depth information, it is difficult to distinguish different shapes perfectly.

10 times smaller object shape by sliding motion. However, for the complicated 3-D shape object, the detection resolution may be a little degraded due to the size difference between sensor and object. Therefore, to get similar haptic information of human, ∼1-mm pitch design (sensor area + spacing) can be recommended considering the density of human's haptic receptors around 100 sites/cm^2. An additional sliding experiment taking into account a soft stamp (PDMS) was carried out in order to analyze the effects of changes in Young's modulus on the stamp [see Fig. 9(e)]. The soft PDMS stamp had complex geometries

with square, triangle, and dome shapes in series. The generated piezoelectric signals from the PDMS stamp had not only increased of noise levels but also a little low SNR value due to its low Young's modulus and the high friction between the PDMS and the polyimide substrate. Due to the change of hardness, the calculated contact width is increased because of a little elastic deformation of PDMS stamp caused by the normal force. Therefore, as like human, we will need to adjust touch force depending on the hardness of touching object.

D. Flexible Sensor Structure and Depth Profile Analysis

Although our piezoelectric sensor array can detect and calculate surface information such as the width of an object or the spacings between objects well, shortcomings exist with regard to depth directions. Unfortunately, as we know, most tactile sensor structures reported so far did not show a good 3-D information for such a small object at the mm level, and even some sensors are limited to detect 2-D information. The main reasons are that the sensor structures are not small sufficiently due to some mechanical design or base materials, which are not enough to flexible. Although specific system such as atomic force microscopy (AFM) or surface profiler (α-step) can give a good depth information, the AFM design is still far from tactile sensor for robot applications. Human skin features such as fingerprints have been studied to enhance the sensing performance in many papers. A fingerprint layer will help to improve the performance of the proposed sensor, but the design and material of the fingerprint layer should be optimized corresponding to the sensor in advance. Instead of using the fingertip like structure, we considered that mimicking the skin deformation could be useful fundamentally to overcome the limits of the sensor first, as humans distinguish the depth information of surfaces well according to the deformation of the skin [31]. Previous experiments positioned the sensor on a hard material such as a desk. Therefore, the sensor could not be deformed sufficiently depending on the shapes of the objects in the depth direction [see Fig. 10(a)]. A soft material was employed on the bottom of the sensor to induce sensor deformation toward the depth direction. The soft material used in this case is a type of sponge similar to PDMS. Therefore, we assumed that Young's modulus of the soft material will be roughly 1 MPa. After applying the soft material, the sliding signals of the three different shapes showed unique characteristics because the sensor deformation for the depth direction had improved. The sensor deformation caused a change in the sliding signal waveform. Small amounts of noise such as signals (the black dotted circles) were noted continuously between the positive and negative peaks for the square shape (see Fig. 10). In the triangle shape, the output voltage was identical to that earlier, but the signal wave form appeared to be sharper and cleaner. The voltage level and signal waveform were also different from those of the dome shape. The sliding signals for the dome shape changed with different output voltages. In the previous experiment, the dome shape led to a point, as in the contact result, whereas the dome shape on the new sensor structure had more contact points with the array sensor, as the pressure levels of each point are different due to the curvature of the dome shape. Although noise-like signal (red dotted circle) was induced by the uneven side of the dome shape, similar to the square shape, the signal wave form easily distinguished the signal from the square shape as well as that from the triangle shape. At this stage, we could distinguish between the three different shapes through the unique characteristics of the sliding signals waveforms. To determine the depth directional information of the various shapes, a signal analysis of the new voltage signals was performed. The edges of the square and triangle shapes are 90° and 60°, respectively, such that the edge tips of both shapes press the sensor cell suddenly and the pressure level remains nearly constant. On the other hand, the dome shape has a circumferential surface such that the applied pressure increases gradually depending on the position of the dome shape after the edge of the dome comes into contact with the sensor cell. These characteristics appeared in the integral values of the piezoelectric voltage signal (see Fig. 10). If the same force is applied suddenly, the accumulated piezoelectric charge values increase rapidly, showing a traditional exponential curve. When the exponential curve is simplified to the form of a line for a simple signal process, the slope values are higher than 0.5 depending on pressure levels in our experiment (0.5–3 N). The integral values for the square and the triangle cases showed a traditional exponential curve when it touched the sensor. The simplified slopes were 0.6 and 0.9, respectively (yellow region). However, for the dome shape, the slope of the integral value was divided into two regions (see Fig. 10). The simplified slope value at these region was 0.2 (blue region), and it then increased to 0.6 (yellow region). Owing to the curved surface of the dome shape, the initial pressure differed from the pressure level of the square or triangle such that the slope of the integral value was low initially. However, the magnitude of the applied pressure increases immediately because the center of the circumferential surface pressed the cell sequentially. The slope change of the integral value was measured in the dome case and could, therefore, be translated as the depth profile. If the array sensor was not deformed enough, there were no slope changes in the dome case. Thus, the main cause of the slope difference of the integral value is the depth change of the sensor layer due to the soft material used.

After applying a soft material to the sensor, the surface topography was assessed, as represented in Fig. 11. The widths of the different shapes were recalculated, as shown in Fig. 11. The recalculated widths of the three shapes also had high accuracy compared to the actual widths. This indicates that the width calculation mechanism using the time interval between the positive and negative peaks is appropriate to obtain the width of the objects, although the signal waveform of the sliding signals was changed. From the slope analysis of the integral value [see Fig. 10(d)], the dome shape could be distinguished from the square and triangle shapes. The depth analysis said that the test sample has two different depth values and it can be interpreted as an inclined form as like dome shape. To get exact depth information, even though some depth information was obtained from the analysis of slop in the integral values of the piezoelectric voltage signal, we need to study more about a matching relation between dynamic piezoelectric voltage level, not peak voltage

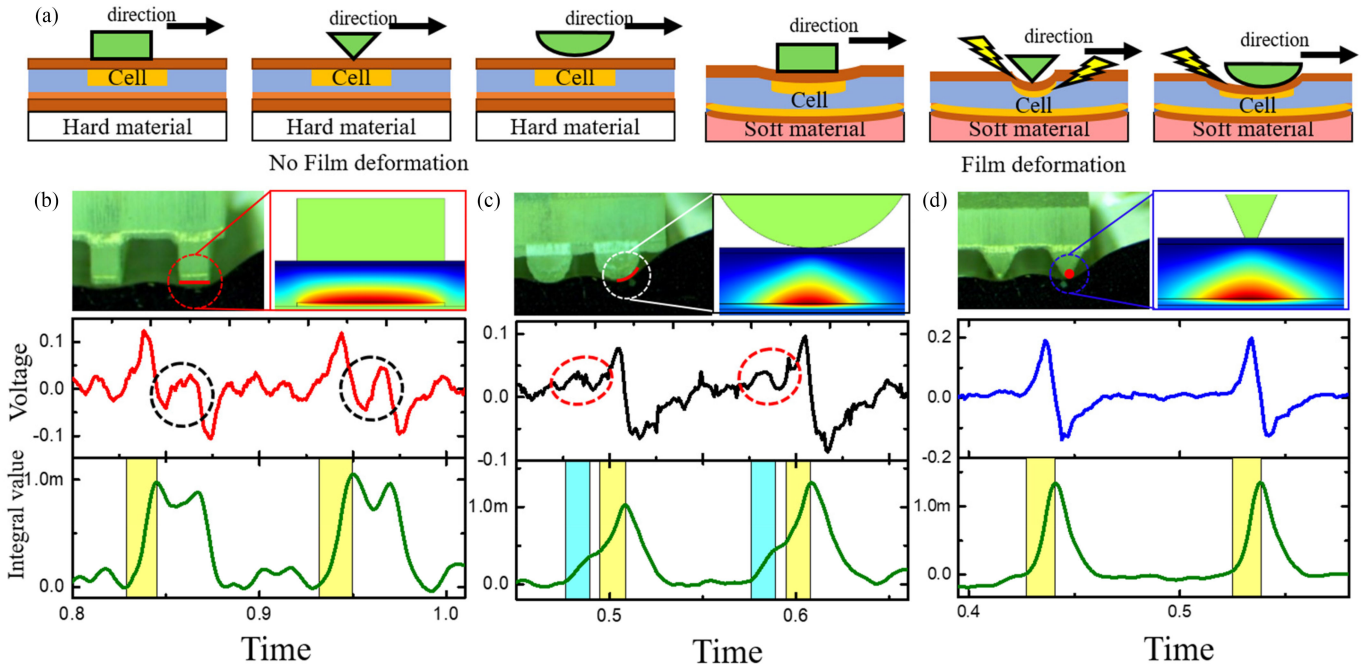

Fig. 10. Sensor deformation mechanism and sliding signals analysis after applying a sponge layer. (a) Deformation distinction between hard and soft materials. (b)–(d) Characteristics of sliding signals after applying a sponge layer and slope analysis of the integral graph (left: square, middle: triangle, and right: dome). Photographs indicate that the sensor was deformed more due to the soft material, and COMSOL simulations represent the piezoelectric potential differences depending on the corresponding shape. Slope analysis of the integral values to obtain the depth profile.

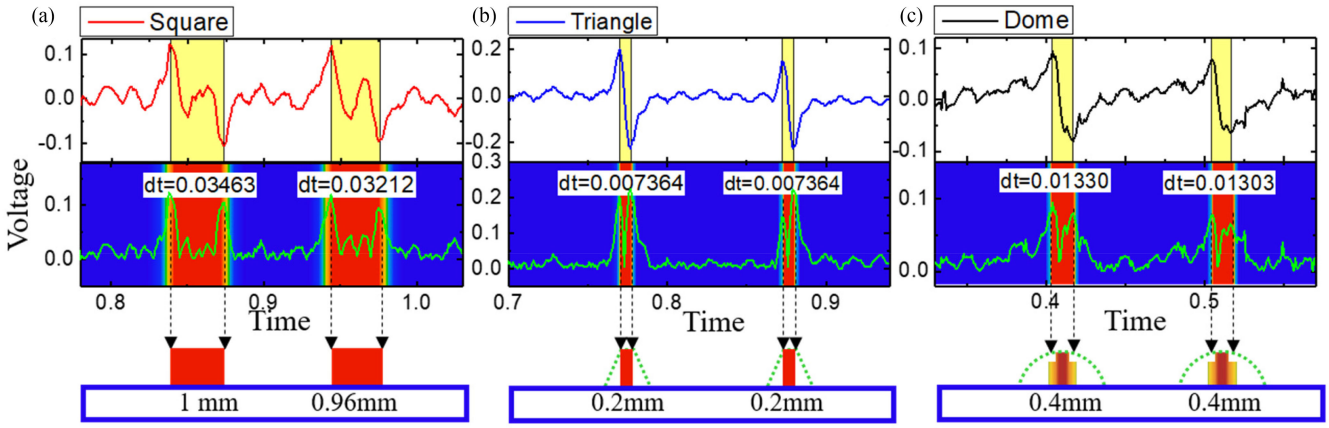

Fig. 11. Representation surface topography from the sliding signals after applying the soft material. The contact width of each shape can be calculated using the time interval between the positive and negative peaks. The calculated width also had high accuracy. The dome shape is able to be distinguished from the other shapes by means of a slope analysis of the integral value.

and pressure value, which can represent the depth shape object. Additionally, although the sensor structure can be deformed by a soft material, the flexibility of sensor structure is not enough to detect depth level of millimetres size small object as the mechanical strength of the polyimide film as the sensor substrate is quite high to resist deformation Therefore, we should modify more the sensor design or materials of sensor body.

V. Conclusion

We proposed a piezoelectric array sensor structure and signal analysis skills for the measurement of surface information such as shape and topography with high accuracy. PVDF-TrFE, a piezoelectric copolymer, was used to create the sensor to measure dynamic movements such as sliding in this case due to its high frequency electromechanical bandwidth and high sensitivity. The suggested array sensor showed high linearity ($R^2 = 0.98$), good reliability (250 times) and stable sensitivity (0.1 V/N). The spatial resolution was four times higher than the resolutions of sensor systems due to the excellent dynamic response of the piezoelectric material and the array design with the detection of variable sliding speeds (10 to 70 mm/s) without a speedometer. With the detected sliding speed, the widths of different shapes could also be calculated precisely compared to the actual surface topography. The piezoelectric sensor with the array design could measure a fine pattern with a 200 μmm width

and a 500 μm pitch despite the fact that the resolution of the sensor is 2 mm. A soft material was applied to the bottom of the piezosensor array to enhance its ability to discriminate between different shapes. A slope analysis of the integral values was done to analyze the depth profile caused by sensor deformation. Eventually, the dome shape could be distinguished from other shapes. Signal processing was optimized and color mapping was applied for the reconstitution of the surface topography.

References

[1] A. Chortos, J. Liu, and Z. Bao, "Pursuing prosthetic electronic skin," *Nature Mater.*, vol. 15, no. 9, pp. 937–950, 2016.

[2] P. Delmas, J. Hao, and L. Rodat-Despoix, "Molecular mechanisms of mechanotransduction in mammalian sensory neurons," *Nature Rev. Neurosci.*, vol. 12, no. 3, pp. 139–153, 2011.

[3] Y. Huang, H. Yuan, W. Kan, X. Guo, C. Liu, and P. Liu, "A flexible three-axial capacitive tactile sensor with multilayered dielectric for artificial skin applications," *Microsyst. Technol.*, vol. 23, pp. 1847–1852, 2007.

[4] Y. Jeong *et al.*, "Psychological tactile sensor structure based on piezoelectric nanowire cell arrays," *RSC Adv.*, vol. 5, no. 50, pp. 40363–40368, 2015.

[5] M. Sim *et al.*, "Structural solution to enhance the sensitivity of a self-powered pressure sensor for an artificial tactile system," *IEEE Trans. Nanobiosci.*, vol. 15, no. 8, pp. 804–811, Dec. 2016.

[6] J. Park, M. Kim, Y. Lee, H. S. Lee, and H. Ko, "Fingertip skin–inspired microstructured ferroelectric skins discriminate static/dynamic pressure and temperature stimuli," *Sci. Adv.*, vol. 1, no. 9, 2015, Art. no. e1500661.

[7] N. T. Tien *et al.*, "A flexible bimodal sensor array for simultaneous sensing of pressure and temperature," *Adv. Mater.*, vol. 26, no. 5, pp. 796–804, 2014.

[8] R. S. Dahiya, G. Metta, M. Valle, and G. Sandini, "Tactile sensing—from humans to humanoids," *IEEE Trans. Robot.*, vol. 26, no. 1, pp. 1–20, Feb. 2010.

[9] H. Yousef, M. Boukallel, and K. Althoefer, "Tactile sensing for dexterous in-hand manipulation in robotics—A review," *Sensors Actuators A, Phys.*, vol. 167, no. 2, pp. 171–187, 2011.

[10] M. Sim *et al.*, "Psychological tactile sensor structure based on piezoelectric sensor arrays," in *Proc. IEEE World Haptics Conf.*, 2017, pp. 340–345.

[11] J. Platkiewicz, H. Lipson, and V. Hayward, "Haptic edge detection through shear," *Sci. Rep.*, vol. 6, 2016, Art. no. 23551.

[12] R. S. Dahiya and M. Valle, *Robotic Tactile Sensing: Technologies and System*. Berlin, Germany: Springer, 2012.

[13] M. Kaneko and K. Tanie, "Contact point detection for grasping an unknown object using self-posture changeability," *IEEE Trans. Robot. Automat.*, vol. 10, no. 3, pp. 355–367, Jun. 1994.

[14] A. A. Stanley, K. Hata, and A. M. Okamura, "Closed-loop shape control of a haptic jamming deformable surface," in *Proc. IEEE Int. Conf. Robot. Automat.*, 2016, pp. 2718–2724.

[15] K. Suwanratchatamanee, M. Matsumoto, and S. Hashimoto, "Robotic tactile sensor system and applications," *IEEE Trans. Ind. Electron.*, vol. 57, no. 3, pp. 1074–1087, Mar. 2010.

[16] S. Dragiev, M. Toussaint, and M. Gienger, "Uncertainty aware grasping and tactile exploration," in *Proc. IEEE Int. Conf. Robot. Automat.*, 2013, pp. 113–119.

[17] J. Scheibert, S. Leurent, A. Prevost, and G. Debrégeas, "The role of fingerprints in the coding of tactile information probed with a biomimetic sensor," *Science*, vol. 323, no. 5920, pp. 1503–1506, 2009.

[18] M. Shimojo and M. Ishikawa, "An active touch sensing method using a spatial filtering tactile sensor," in *Proc. IEEE Int. Conf. Robot. Automat.*, 1993, pp. 948–954.

[19] V. Maheshwari and R. F. Saraf, "High-resolution thin-film device to sense texture by touch," *Science*, vol. 312, no. 5779, pp. 1501–1504, 2006.

[20] M. L. Hammock, A. Chortos, B. C. K. Tee, J. B. H. Tok, and Z. Bao, "25th anniversary article: The evolution of electronic skin (E-Skin): A brief history, design considerations, and recent progress," *Adv. Mater.*, vol. 25, no. 42, pp. 5997–6038, 2013.

[21] Z. L. Wang and J. Song, "Piezoelectric nanogenerators based on zinc oxide nanowire arrays," *Science*, vol. 312, no. 5771, pp. 242–246, 2006.

[22] H. Athenstaedt, H. Claussen, and D. Schaper, "Epidermis of human skin: pyroelectric and piezoelectric sensor layer," *Science*, vol. 216, no. 4549, pp. 1018–1020, 1982.

[23] L. Pinna, A. Ibrahim, and M. Valle, "Interface electronics for tactile sensors based on piezoelectric polymers," *IEEE Sensors J.*, vol. 17, no. 18, pp. 5937–5947, Sep. 2017.

[24] M. Di Donato, "Development of composite piezoelectric materials for tactile sensing," Politecnico di Torino, 2015.

[25] P. T. Hoang, H. Phung, C. T. Nguyen, T. D. Nguyen, and H. R. Choi, "A highly flexible, stretchable and ultra-thin piezoresistive tactile sensor array using PAM/PEDOT: PSS hydrogel," in *Proc. 14th Int. Conf. Ubiquitous Robots Ambient Intell.*, 2017, pp. 950–955.

[26] R. Rocha, P. Lopes, A. T. de Almeida, M. Tavakoli, and C. Majidi, "Soft-matter sensor for proximity, tactile and pressure detection," in *Proc. IEEE/RSJ Int. Conf. Intell. Robots Syst.*, 2017, pp. 3734–3738.

[27] Y.-C. Chung, S.-T. Chuang, T.-Y. Chen, C.-Y. Lo, and R. Chen, "Capacitive tactile sensor for angle detection and its accuracy study," *IEEE Sensors J.*, vol. 16, no. 18, pp. 6857–6865, Sep. 2016.

[28] S.-J. Woo, J.-H. Kong, D.-G. Kim, and J.-M. Kim, "A thin all-elastomeric capacitive pressure sensor array based on micro-contact printed elastic conductors," *J. Mater. Chem. C*, vol. 2, no. 22, pp. 4415–4422, 2014.

[29] M. Kaltenbrunner *et al.*, "An ultra-lightweight design for imperceptible plastic electronics," *Nature*, vol. 499, no. 7459, pp. 458–463, 2013.

[30] M. Mukaka, "A guide to appropriate use of Correlation coefficient in medical research," *Malawi Med. J.*, vol. 24, no. 3, pp. 69–71.

[31] P. Isokoski and J. Springare, *Haptics: Perception, Devices, Mobility, and Communication: 8th International Conference, EuroHaptics 2012, Tampere, Finland, June 13-15, 2012 Proceedings*. Berlin, Germany: Springer, 2012.

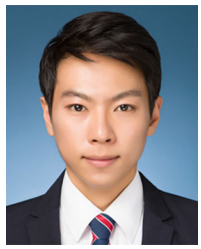

Kwonsik Shin received the B.S. degree in semiconductor science and technology from Chonbuk National University, Jeonju, South Korea, in 2015 and the M.S. degree in electrical devices for artificial tactile sensor and neural probes, in 2017 from Daegu Gyeongbuk Institute of Science and Technology, Daegu, South Korea, where he is currently working toward the Ph.D. degree in electrical devices for artificial tactile sensor and neural probes.

Since 2015, he has been with the Department of Information and Communication Engineering, Daegu Gyeongbuk Institute of Science and Technology.

Minkyung Sim received the B.Eng. degree in electronics engineering from Kyungpook National University, Daegu, South Korea, in 2013. He is currently working toward the integrated M.Eng. and Ph.D. degrees in information and communication engineering at Daegu Gyeongbuk Institute of Science and Technology, Daegu, South Korea.

Eunmin Choi received the B.S. degree in electronics engineering from Kyungpook National University, Daegu, South Korea, in 2014 and the M.S. degree in vehicle networks and vehicular security, in 2017 from Daegu Gyeongbuk Institute of Science and Technology, Daegu, South Korea, where she is currently working toward the Ph.D. degree in vehicle networks and vehicular security.

Since 2015, she has been with the Department of Information and Communication Engineering, Daegu Gyeongbuk Institute of Science and Technology.

Hyunchul Park received the B.S. degree in electronic engineering from Kyungpook National University, Daegu, South Korea, in 2016 and the M.S. degree in information and communication engineering from Daegu Gyeongbuk Institute of Science and Technology, Daegu, South Korea, in 2018.

He is currently a CS in ASML.

Ji-Woong Choi (S'00–M'04–SM'09) received Ph.D. degree from Seoul National University (SNU), Seoul, South Korea, in 2004.

From 2005 to 2007, he was a Postdoctoral Visiting Scholar with the Department of Electrical Engineering, Stanford University, Stanford, CA, USA. He was also a Consultant with GCT Semiconductor, San Jose, CA, USA, for development of mobile TV receivers from 2006 to 2007. Since October 2010, he has been with the Department of Information and Communication Engineering, Daegu Gyeongbuk Institute of Science and Technology, Daegu, South Korea, as an Associate Professor. His research interests include wireless communication theory, signal processing, biomedical communication applications, and brain–machine interface.

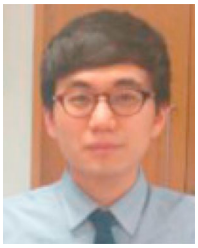

Yuljae Cho received the Ph.D. degree in engineering science from University of Oxford, Oxford, U.K., in 2018.

His research interests include environmental energy harvesting through the photovoltaic effect and piezo-/triboelectric effects.

Jung Inn Sohn is currently a Professor with the Division of Physics, Department of Semiconductor Science, Dongguk University, Seoul, South Korea. He was formerly a Senior Researcher with the University of Oxford (2013–2017), Samsung Advanced Institute of Technology (2011–2012), and the University of Cambridge (2005–2010). His research interests include fabrication of new nanomaterials, exploration of their physical properties and new functions, and the development of novel nanoscale devices with a view to potential processing, and fabrication routes.

Seung Nam Cha received the Ph.D. degree in electrical engineering from the University of Cambridge, Cambridge, U.K., in 2006.

He is currently an Associate Professor with the Physics Department, Sungkyunkwan University, Seoul, South Korea, and was a Principal Researcher with Samsung Advanced Institute of Technology (1996–2012) and an Associate Professor in engineering science with the University of Oxford (2014–2018). He has extensive research experience in the area of nanoelectronics, energy harvesting, and display/lighting system.

Jae Eun Jang received the Ph.D. degree in electrical engineering from the University of Cambridge, Cambridge, U.K., in 2006.

From 2007 to 2011, he was a Principal Senior Researcher with Samsung Advanced Institute of Technology, Yongin, South Korea. Since 2011, he has been a Professor in information and communication engineering with Daegu Gyeongbuk Institute of Science and Technology, Daegu, South Korea. His research interests include electrical devices for bioapplications or ultra high frequency region.